Chemical reactions of conformationally selected 3-aminophenol molecules in a beam with Coulomb-crystallized Ca$^+$ ions

Daniel Rösch, Stefan Willitsch, Yuan-Pin Chang, and Jochen Küpper

---

Articles you may be interested in

Coherent or hopping like energy transfer in the chlorosome ?
The Journal of Chemical Physics **1610**, (2015); 10.1063/1.4893524

Fast generation of domain walls with defined chirality in nanowires
The Journal of Chemical Physics **104**, 172404172404 (2014); 10.1063/1.4874803

Tunable eigenmodes of coupled magnetic vortex oscillators
The Journal of Chemical Physics **104**, 182405182405 (2014); 10.1063/1.4875618

Local modification of the magnetic vortex-core velocity by gallium implantation
The Journal of Chemical Physics **115**, 103909103909 (2014); 10.1063/1.4868222

Dynamic coupling of magnetic resonance modes in pairs of mesoscopic rectangles
The Journal of Chemical Physics **114**, 043905043905 (2013); 10.1063/1.4813870

Time structure of fast domain wall creation by localized fields in a magnetic nanowire
The Journal of Chemical Physics **103**, 092406092406 (2013); 10.1063/1.4819729

Chemical reactions of conformationally selected 3-aminophenol molecules in a beam with Coulomb-crystallized Ca$^+$ ions

Daniel Rösch,[1] Stefan Willitsch,[1,a)] Yuan-Pin Chang,[2] and Jochen Küpper[2,3,4,b)]

[1]*Department of Chemistry, University of Basel, Klingelbergstrasse 80, 4056 Basel, Switzerland*
[2]*Center for Free-Electron Laser Science, DESY, Notkestrasse 85, 22607 Hamburg, Germany*
[3]*Department of Physics, University of Hamburg, Luruper Chaussee 149, 22761 Hamburg, Germany*
[4]*The Hamburg Center for Ultrafast Imaging, University of Hamburg, Luruper Chaussee 149, 22761 Hamburg, Germany*

Many molecules exhibit multiple conformers that often easily interconvert under thermal conditions. Therefore, single conformations are difficult to isolate which renders the study of their distinct chemical reactivities challenging. We have recently reported a new experimental method for the characterization of conformer-specific effects in chemical reactions [Y.-P. Chang, K. Długołęcki, J. Küpper, D. Rösch, D. Wild, and S. Willitsch, "Specific chemical reactivities of spatially separated 3-aminophenol conformers with cold Ca$^+$ ions," Science **342**, 98–101 (2013)]. Different conformers are spatially separated using inhomogeneous electric fields and reacted with a Coulomb crystal of cold, spatially localized ions in a trap. As a first application, we studied reactions between the two conformers of 3-aminophenol and Ca$^+$. We observed a twofold larger rate constant for the *cis* compared to the *trans* conformer which was rationalized in terms of the differences in the long-range ion-molecule interactions. The present article provides a detailed description of the new method and a full account of the experimental results as well as the accompanying theoretical calculations. © 2014 AIP Publishing LLC. [http://dx.doi.org/10.1063/1.4869100]

I. INTRODUCTION

Many molecules possess multiple conformers (rotational structural isomers) that interconvert with low energy barriers through hindered rotations about single covalent bonds. It is well known that different conformations can exhibit distinct chemical reactivities.[1–3] To gain a comprehensive understanding of the chemical behavior of molecules, it is thus necessary to investigate their conformer-specific chemistry. To this end, individual molecular conformations need to be isolated and characterized. Moreover, the capability to manipulate conformational distributions provides means to influence reactivities and products, adding to the repertoire of methods to control chemical processes.

When studies of conformational effects are carried out at low temperatures in the gas phase, the thermal interconversion of conformations is suppressed. In recent years, significant progress toward the spectroscopic characterization of specific conformations has been achieved.[4–13] For instance, studies of photoinduced ground-state isomerization reactions mapped out interconversion pathways between conformations, i.e., minima on the corrugated potential energy surfaces.[14–16] Investigations of the conformational landscape of small molecules, e.g., poly-aminoacids, helped to understand the folding motives in peptides.[10]

Unimolecular conformer-specific dynamics have been investigated in the photodissociation of cations of small organic molecules.[17–19] In these studies, individual conformers of cations were selectively generated capitalizing on the different ionization energies of their parent neutrals. In addition, photodissociation studies on neutral conformers of small organic molecules have been carried out.[20–22] In these studies, individual conformers were not separated prior to photoexcitation. Consequently, the experimental results contained contributions from all populated conformations. These were disentangled through Rydberg tagging methods which allowed for resolving the small energy difference between conformers manifested in the kinetic energy release of H photofragments.

For bimolecular reactions in the gas phase only few investigations of conformational effects have been reported so far. Taatjes *et al.*[23] observed conformer-dependent reactivities from the simplest Criegee intermediate (CH$_3$OO) which plays a key role in ozonolysis reactions. In a cryogenic matrix, Khriachtchev *et al.*[24] observed distinct conformer-dependent products from two formic acid conformers reacting with oxygen atoms.

Several techniques for the manipulation of conformational distributions of molecules in the gas-phase have been reported. Ion mobility allows the separation of molecules according to their shape and thus serves as a key technique to separate classes of conformers of large charged molecules.[25] For neutral molecules, the spatial separation of specific conformers has been achieved using electric fields.[26–28] While all conformers of a molecule have the same mass, they often differ by their dipole moments. Different dipole moments lead to different Stark shifts of rotational energy levels in electric fields. Thus, in an inhomogeneous electric field different forces act on the different conformers, which can be used for the manipulation of their translational motion.

a)Electronic mail: stefan.willitsch@unibas.ch
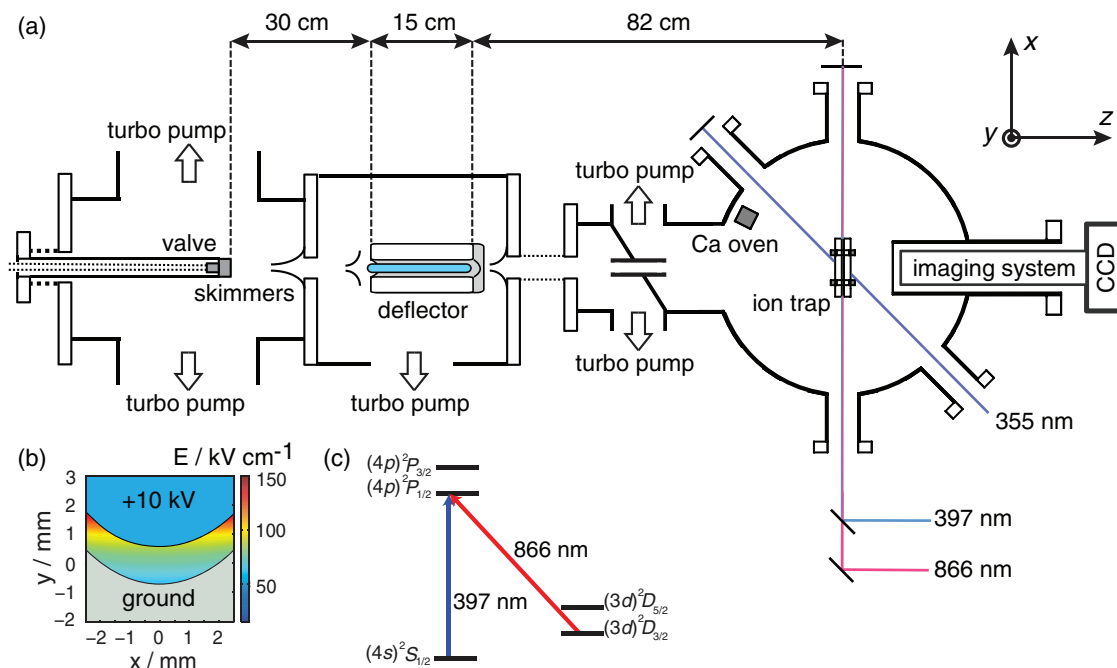b)Electronic mail: jochen.kuepper@cfel.de

FIG. 1. (a) Schematic top view of the experimental setup for studying conformer-selected chemical reactions. See text for details. (b) Electric field strength E along a cut through the electrostatic deflector. (c) Diagram of energy levels accessed during Doppler laser cooling of $^{40}Ca^+$.

Recently, we have adapted this technique to investigate the chemical reactivities, i.e., rate constants, of specific conformers in the prototypical bimolecular reactions of 3-aminophenol (3AP) and Ca^+.[29] 3AP has two stable conformers (denoted *cis* and *trans*) which differ in the orientation of the OH group and have significantly different dipole moments (2.33 D and 0.77 D for the *cis*- and *trans*-species, respectively).[47,56] 3AP was entrained in a molecular beam and spatially separated using the electrostatic deflector. The dispersed molecular beam was directed at a stationary reaction target consisting of a Coulomb crystal of Ca^+ ions, i.e., an ordered structure of translationally cold ions at a temperature of a few millikelvins in a trap.[30] Singly ionized Ca ions were chosen as a co-reactant because they can easily be Coulomb-crystallized by laser cooling. Ca^+ is also known for its reactivity with organic molecules acting as a catalyst for the activation of inert chemical bonds[31,32] such as C–F and C–O.[33–35]

In the present article, we give a detailed account of our methods and results on the conformer-specific reactivities of 3AP with Ca^+. The outline of the paper is as follows: Secs. II and III describe the experimental setup and theoretical procedures employed. In Sec. IV, we present a characterization of the electrostatic deflection of the conformers, their reaction profiles, conformer-specific reaction rate constants as well as mass spectra of the reaction products. An analysis of the results based on theoretical calculations follows in Sec. V.

II. EXPERIMENTAL SETUP

The experimental setup consists of two main parts: a molecular beam deflection apparatus for the separation of 3AP conformers and an ion trap apparatus for the generation and storage of Coulomb crystals of laser cooled Ca^+

ions. The individual experimental procedures have been reported previously.[27,29,30,36,37] In the following, we focus on the details of the combined apparatus and the methodology for conformer-specific reaction experiments.

A. Conformer deflection setup

The molecular beam machine for conformer deflection consisted of a series of differentially pumped vacuum chambers. The source chamber housing a pulsed valve was pumped by two 1650 l/s turbomolecular pumps. The deflector chamber containing the electrostatic deflector was pumped by a 500 l/s turbomolecular pump, as shown in Figure 1(a). A solid sample of 3AP (Sigma-Aldrich, 98%) was placed in a reservoir cartridge and vaporized at 145 °C inside a high-temperature Even-Lavie valve.[38] The valve was operated at a backing pressure of 35 bars of neon at a repetition rate of 600 Hz. The typical rotational temperature of 3AP in our experiments was about 1 K. Two skimmers with diameters of 2 mm and 1 mm were placed 15 cm and 27 cm downstream from the nozzle, respectively. After skimming, the collimated molecular beam entered the 15 cm long electrostatic deflector.[39–42] A cut through the electrodes of the deflector including a contour plot of the generated electric field is shown in Figure 1. The vertical gap between the deflector electrodes perpendicular to the molecular beam axis was 1.4 mm. The shape of the electrodes was designed to generate a strong inhomogeneous electric field with a nearly constant gradient along the y axis.[39,40] The molecular beam passed a third skimmer with a diameter of 1.5 mm for differential pumping into a chamber pumped by a 345 l/s turbomolecular pump. Subsequently, the beam entered the reaction chamber, pumped by a 550 l/s turbomolecular pump, through another differential pumping

aperture formed by a 3.5 cm long, 10-mm-diameter tube. Typical pressures during the experiments were 7×10^{-6} mbar, 9×10^{-8} mbar, and 2×10^{-9} mbar in the source, deflector, and reaction chambers.

B. Ion trap setup

In the reaction chamber, Coulomb crystals of laser-cooled Ca^+ ions were generated and trapped in a linear radiofrequency (RF) ion trap.[30,37] Ca^+ ions were produced by non-resonant multi-photon ionization of a beam of Ca atoms evaporated from an oven and passing through the center of the ion trap,[30,43] see Figure 1(a). The ion trap consisted of four segmented cylindrical electrodes with a radius $r = 4.0$ mm arranged in a quadrupolar configuration. To confine the ions in the plane perpendicular to the trap symmetry axis, RF voltages with amplitudes $V_{0,RF} = 350$ V and frequencies $\Omega = 2\pi \times 3.1$ MHz were applied with opposite polarities across adjacent electrodes. To confine the ions along the axis, static voltages in the range of $V_{end} = 1–10$ V were applied to the endcap electrodes. The atomic beam was ionized using the third harmonic (355 nm) of a Nd:YAG laser close to the center of the ion trap. The Ca^+ ions were laser-cooled with beams produced by two external cavity enhanced diode lasers operating at wavelengths of 397 nm and 866 nm to pump the $(4s)^2S_{1/2} \rightarrow (4p)^2P_{1/2}$ and $(3d)^2D_{3/2} \rightarrow (4p)^2P_{1/2}$ transitions, respectively,[30] see Figure 1(c). The frequencies of the two laser beams were simultaneously monitored using an automated fiber-switcher coupled to a wavemeter and stabilized by a computer-controlled voltage feedback loop. The resulting laser linewidths were on the order of a few MHz. The laser powers employed were about 600 μW and 200 μW for the 397 nm and 866 nm beams, respectively. Upon laser cooling, the ions localized in space and formed three-dimensional spheroidal Coulomb crystals[30,37] with a radius $r \approx 100$ μm and a width $x \approx 550$ μm typically consisting of $\sim$700 ions. The secular kinetic energy of the laser cooled ions amounted to $E_{sec} \approx k_B \times 10$ mK. Two-dimensional cuts of the central plane of the Coulomb crystals were imaged by collecting a solid angle of the atomic fluorescence generated during laser cooling using an enhanced CCD camera coupled to a microscope with tenfold magnification.

C. Reaction rate measurements

The first step in each reaction experiment consisted of the formation of a Coulomb crystal. Subsequently, the molecular beam valve was switched on to admit pulse trains of deflected 3AP molecules to collide and react with the spatially localized ions. Different parts of the deflected molecular beam were directed at the stationary Coulomb crystal reaction target by tilting the molecular beam setup in the y direction using a translational stage with a precision of 10 μm. The width of deflection coordinates sampled by the ion cloud was defined by the y extension of the Coulomb crystals, i.e., 200 μm. Ions that reacted with 3AP formed product ions which remained trapped, but were not laser cooled and, therefore, did not fluoresce.[44] These product ions were sympathetically cooled by the re-

maining Ca^+ ions to form a dark shell around the crystal. The progress of the reaction was monitored by observing the shrinking of the bright fluorescing Ca^+ core of the Coulomb crystals as a function of time. Images of the crystals were recorded every 30 s with a camera shutter time of 0.4 s over reaction times of typically 8 to 15 min. From the recorded images, the number of unreacted Ca^+ ions as a function of time was determined from the crystal volumes.[44] Note that the 3AP molecules in the reaction volume were replenished with each gas pulse. Therefore, their number density was essentially constant during the measurement time and the decrease of the number $N(t)$ of Ca^+ ions in the crystal as a function of time t followed pseudo-first-order kinetics. Pseudo-first-order reaction rate constants k_1 were determined at specific deflection voltages and deflection coordinates y according to the rate law

$$\ln \frac{N(y,t)}{N(y,t=0)} = -k_1(y)t. \qquad (1)$$

The deflection coordinate y is defined as the offset of the deflected from the nominally undeflected beam at the position of the Coulomb crystal. All measurements were performed with the same power and detuning of the cooling laser from resonance to ensure a constant and well-defined population of all three electronic levels of Ca^+ accessed during laser cooling (see Figure 1(c)). The populations of the relevant Ca^+ states were determined from a calibrated eight-level optical Bloch equation treatment including the effects of magnetic fields.[45]

Reactions with residual background H_2 gas in the ion trap chamber also contributed to a removal of Ca^+ ions from the trap. The corresponding loss rates were measured for each set of experiments following the same procedures described as above but without admitting the molecular beam. The resulting values for the background loss rates were subtracted from the measured rates in the actual reaction experiments. We note that collisions with the Ne carrier gas of the molecular beam did not lead to any observable loss of Ca^+ ions from the trap, as confirmed by control experiments with pure Ne beams.

D. Mass spectrometry of trapped ions

The ionic reaction products were analyzed using resonant-excitation (RE) mass spectrometry of the Coulomb crystals.[37,45] Here, the motion of specific ion species was resonantly excited by scanning the frequency of an additional RF drive voltage (0.2–0.3 V) applied to one of the trap electrodes. When the RF field was resonant with the motional frequency of a trapped ion species, the Coulomb crystal heated up. This led to a dislocation of the Ca^+ ions from their equilibrium position. RE mass spectra were recorded by slowly scanning the excitation frequency while monitoring the increase of the fluorescence yield in a region close to but outside the normal extent of the Coulomb crystal. RE mass spectra of multi-component crystals generally show broad peaks that are shifted with respect to single-species crystals.[46] The exact intensity and position of the features depends on the scan speed, the drive amplitude, the scan direction, and the crystal composition. Therefore, RE mass spectrometry only allows an

approximate determination of the masses of the species present in a multi-component Coulomb crystal.[45]

E. Molecular beam profile measurements

Spatial deflection profiles of 3AP were recorded in a time-of-flight (TOF) mass spectrometer that replaced the ion-trap apparatus. 3AP molecules were ionized at the same distance from the deflector as the ion trap via resonance-enhanced two-photon ionization (R2PI) by a frequency-doubled pulsed dye laser pumped by a Nd:YAG laser with a repetition rate of 20 Hz. Pulses of 10 ns duration with an energy of approximately 0.4 mJ were focused to a spot size of 240 μm in the interaction volume. The molecular ions were mass-selectively detected by their arrival time on a multi-channel-plate (MCP) detector. *cis*- and *trans*-3AP were differentiated through their distinct excitation wavenumbers of 34 109 cm^{-1} and 34 467 cm^{-1}, respectively.[47]

III. THEORETICAL AND COMPUTATIONAL METHODS

A. DFT calculations of reaction paths on the ground-state potential energy surface

Short-range ion-molecule interactions were investigated computationally using density functional theory (DFT) calculations. Stationary points along reaction paths to two possible products were computed at the DFT MPW1K/cc-pVTZ level of theory, using the Gaussian 09 software suite.[48–50] Transition state structures were calculated by a quadratic-singular-transit approach (QST-3),[51,52] from energy-minimized Ca$^+$-3AP and Ca$^+$-product-radical complexes and an initial transition state guess. To verify convergence to a saddle point, the resulting transition state structure was distorted and re-submitted as a starting point in a new QST-3 calculation for the transition state search. Basis set superposition errors were corrected using the counterpoise routine provided in Gaussian 09.

B. Adiabatic capture theory

Long-range ion-molecule capture kinetics were modeled using the adiabatic capture theory developed by Clary and co-workers.[53,54] The long-range interaction potential V between an ion and a polar molecule was approximated by the sum of the dominant charge-permanent dipole[55] and charge-induced dipole interactions

$$V(R, \beta) = -\frac{q\mu_D \cos\beta}{R^2} - \frac{q^2\alpha}{2R^4}, \qquad (2)$$

where R is the distance between the ion and the center of mass of the 3AP molecule, μ_D is its permanent electric dipole moment,[55,75] β the orientation angle of the molecular dipole moment with the ion-molecule axis, q the charge of the ion, and α the scalar polarizability of 3AP. Using the methods described in Ref. 54, centrifugally corrected and rotationally adiabatic potential energy curves for the system Ca$^+$ + *cis-/trans*-3AP were calculated for 3AP rotational states with quantum numbers ranging from $j = 0$ to $j = 100$

for R between 2 and 48 a$_0$. The dipole moments of 3AP were taken from Ref. 56, the isotropic polarizabilities were calculated at the DFT B3LYP/aug-cc-pVTZ level of theory. Rotational-state-specific reaction cross sections for $j = 0$ up to $j = 15$ were calculated from a summation over all partial waves for which the maximum of the centrifugally corrected potential energy curve did not exceed the experimental collision energy. Effective capture rate constants were calculated by multiplying the state-specific cross sections with the velocity and the relevant state populations at the rotational temperature of 3AP in the molecular beam.

C. Molecular-dynamics simulations of Coulomb crystals

Fluorescence images and RE mass spectra of the multi-component Coulomb crystals were simulated using molecular dynamics (MD) methods. MD simulations were performed using a modified version of the Protomol program package.[57] Fluorescence images were simulated from ion trajectories calculated by solving the classical three-dimensional equations of motion of the ions in the trap under the influence of laser cooling.[37,58] To minimize computer time, an isotropic friction force to emulate laser cooling and the pseudopotential approximation for the ion trap was used.[30] RE mass spectra were simulated following the methods described in Refs. 45 and 46. Briefly, the Coulomb crystals were offset from the central trap axis by 20 μm at the beginning of the simulation and allowed to relax. The Fourier transform of the time-dependent total kinetic energy of the ions yielded the frequency spectrum of the Coulomb crystal which is also the experimental observable. The frequencies obtained by this method were calibrated using a comparison of a measured and calculated RE mass spectrum of a pure Ca$^+$ crystal. A correction factor of 0.92 was applied to the calculated frequencies of each spectrum to achieve optimal agreement with the experiment.

D. Monte Carlo simulations of molecular beam profiles

The simulation of spatial deflection profiles has been described in detail previously.[36,59] Briefly, the electric field E and its gradient ($\vec{\nabla}E$) were calculated using finite element methods implemented in the COMSOL Multiphysics program. Stark energy curves $W(E)$ of the 3AP quantum states and their effective dipole moments μ_{eff} were calculated using CMIstark[60] (see Figure 2). From the electric fields and Stark energy curves, the molecular beam deflection profiles were calculated with libcoldmol.[36] Trajectories for molecules in individual rotational quantum states were obtained by numerical integration of the 3D equations of motion using a Runge-Kutta algorithm. The initial conditions according to the parameters of the molecular beam were sampled by a Monte Carlo approach, and every individual molecule was propagated through a simulated beamline that includes all mechanical apertures of the experimental setup.

The spatial deflection profile $I(y, T_{\text{rot}})$ for an ensemble of molecules at a rotational temperature T_{rot} was calculated from
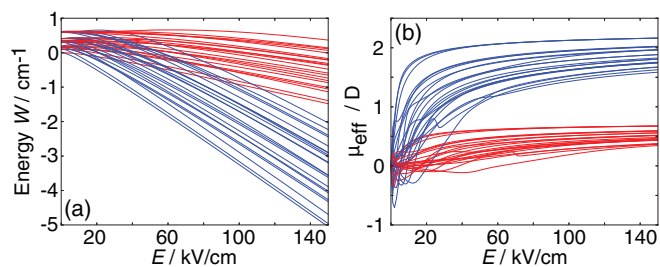
FIG. 2. (a) Stark energies W for the lowest rotational quantum states $j = 0$–2 of (blue) *cis*- and (red) *trans*-3AP as a function of the electric field strength E. (b) Effective dipole moments μ_{eff} for $j = 0$–2 of *cis*- (blue) and *trans*- (red) 3AP.

the single-quantum-state deflection profiles $I_s(y)$ using

$$I(y, T_{\mathrm{rot}}) = \frac{1}{w} \sum_{s=1}^{N} w_s(T_{\mathrm{rot}}) I_s(y). \qquad (3)$$

Here, N is the number of quantum states included in the simulation and $w_s(T_{\mathrm{rot}}) = g_M g_{\mathrm{ns}} e^{(W_0 - W_s)/(k_B T_{\mathrm{rot}})}$ is the population weight for a given quantum state. W_0 is the field-free energy of the ground state and W_s the field-free energy of state s. $g_M = 1$ for $M = 0$ and $g_M = 2$ otherwise. g_{ns} accounts for nuclear spin statistical weight of the current state with $g_{\mathrm{ns}} = 1$ for all rotational states of 3AP. The normalization constant is given by $w = \sum_{s=1}^{N} w_s$.

IV. EXPERIMENTAL RESULTS

A. Deflection curves of 3AP

The density of each conformer in the deflected and dispersed molecular beam was measured by recording the number of R2PI-ionized *cis* and *trans* conformers of 3AP as a function of the deflection coordinate y. The measured conformer-selective deflection profiles are shown in Figure 3, in which each data point represents the signal averaged over 1000 laser shots. When high voltages were applied to the deflector, both conformers were deflected upwards. The deflection was considerably larger for the more polar *cis*-3AP. For instance, for a deflector voltage of 7.5 kV above $y = 6$ mm a pure sample of *cis* conformers was obtained (see Figure 3(b)). The insets in Figure 3 show that the fraction of *cis*-3AP in the probed sample can be continuously tuned as a function of y. At heights above the cut-off of the *trans*-3AP beam profile, the density of the *cis* conformers is still comparable to its density in the free jet, i.e., it is only decreased to one fourth. When increasing the voltages to 13 kV (Figure 3(d)), *cis*-3AP was deflected so strongly that it was essentially depleted from the detection region. As a consequence, an almost clean sample of *trans*-3AP was obtained.

Monte Carlo simulations of the deflection curves are shown as solid lines in Figure 3. The simulations at an initial rotational temperature of 1.1 K agree well with the experimental profiles. In particular, the fractional intensities plotted in the insets were reproduced by the simulations (solid lines). The simulated profiles and the measured population ratios of the two conformers were used for fitting conformer-
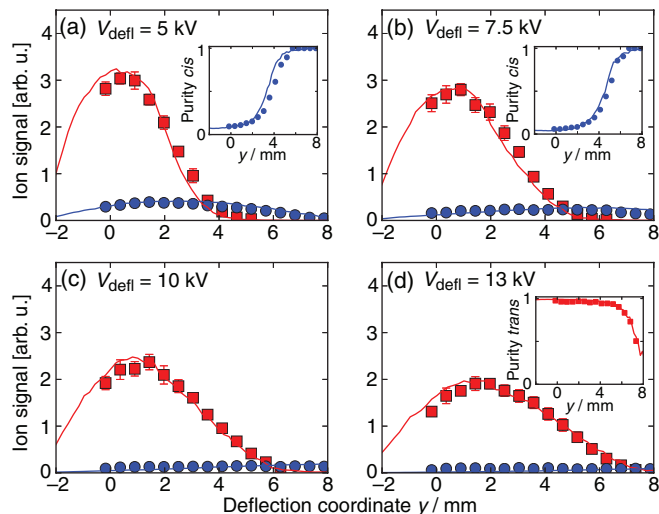

FIG. 3. Density profiles of the deflected beam of *cis* (blue) and *trans* (red) 3AP at deflector voltages $V_{\mathrm{defl}} =$ (a) 5 kV, (b) 7.5 kV, (c) 10 kV, and (d) 13 kV. These data were measured by conformer-specific multi-photon ionization as a function of the molecular-beam deflection coordinate y. Solid lines: corresponding Monte Carlo trajectory simulations. In the insets, purities of (a) and (b) *cis* and (d) *trans* conformers are given, as obtained by dividing the relevant conformer density profile by the sum of the *cis* and *trans* profiles. Error bars indicate the statistical 95% confidence interval of the data points.

specific rate constants from measured reaction rate profiles as described in Sec. IV C.

For the simulated deflection profiles shown in Figure 3, different rotational states with rotational angular momentum quantum numbers j have different spatial distributions according to their different effective dipole moments μ_{eff}. Figure 4 shows the simulated deflection profiles of individual states ranging from $j = 0$ to $j = 8$. For each profile, the contribution of all j_τ states weighed with their relative thermal populations at the rotational temperature of 1.1 K and their statistical weights were included. τ denotes the asymmetric top projection quantum number. Thus, the area underneath each j
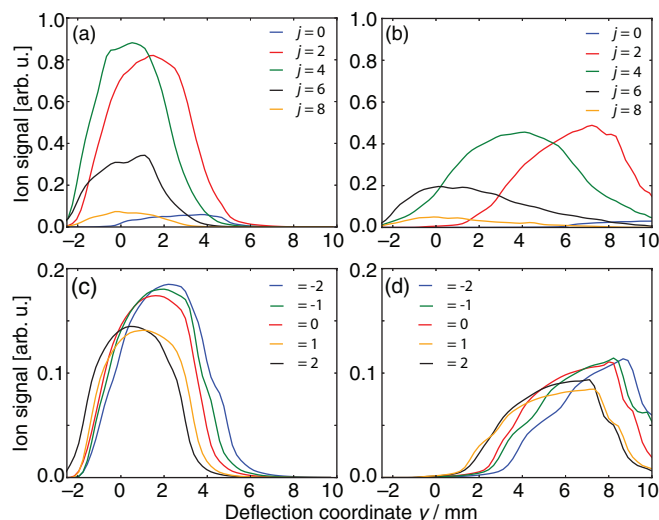

FIG. 4. Deflection profile simulations at $V_{\mathrm{defl}} = 7.5$ kV for even $j = 0$ to $j = 8$ for specific rotational states j of (a) *trans*- and (b) *cis*-3AP, and for specific asymmetric-top quantum numbers τ at $j = 2$ of (c) *trans*- and (d) *cis*-3AP. See text for details.

profile in Figure 4 represents the relative thermal population of each j manifold at 1.1 K as well as their relative contribution to the reactions. Comparing the deflection profiles of individual j states for the two conformers, profiles of low j of *cis*-3AP exhibit significantly stronger spatial deflection than those of *trans*-3AP. However, for high j states both conformers show similar deflection patterns demonstrating the quickly vanishing dipole moment for rotationally excited species and the need for very cold molecular beams.[28]

B. Number density of 3AP

The absolute number density of 3AP in the molecular beam was derived by calibration against the reaction $N_2O + Ca^+ \rightarrow CaO^+ + N_2$. From measurements of the pseudo-first-order rate constants for this reaction and the reported value for the second-order-rate constant,[61] the density of N_2O molecules in the beam was determined. The ratio of the experimentally determined first order rate constant to the known second order rate constant was equivalent to the time-averaged number density n_{avg}. For $k_1 = 4.30(4) \times 10^{-3} \, s^{-1}$, measured with a beam of 50 mbar of N_2O seeded in 30 bars of Ne we obtained $n_{avg}(N_2O) = 3.84(62) \times 10^7 cm^{-3}$. Assuming that the number densities in the beam were proportional to the partial pressures before expansion (for 3AP at 145 °C approximately 10 mbar[62]), the 3AP density was estimated to be $n_{avg} = 7.7(12) \times 10^6 \, cm^{-3}$.[63]

C. Reaction profiles and conformer-specific rate constants of Ca⁺ + 3AP

In Figure 5, the experimentally determined pseudo-first-order rate constants $k_{1,total}$ are shown as a function of deflection coordinate y for four deflector voltages $V_{defl} = 5, 7.5, 10,$ and 13 kV. Each data point in Figure 5 represents the mean of at least four individual reaction measurements. The measured

rate constants $k_{1,total}(y)$ reflect both, the density distributions of conformers in the deflected molecular beam $n_{trans/cis}$ and the conformer-specific second-order rate constants $k_{2, trans/cis}$ of the reaction:

$$k_{1,total}(y) = k_{2,cis}n_{cis}(y) + k_{2,trans}n_{trans}(y), \qquad (4)$$

where $n_{trans}(y)$ and $n_{cis}(y)$ were determined as described in Sec. IV A. The population weighted-rate constants $k_{2, cis}$ and $k_{2, trans}$ were determined from a global fit of (4) to the reaction-rate profiles in Figure 5. The fit yielded the conformer-specific rate constants $k_{2, cis} = 2.3(9) \times 10^{-10} cm^3 \, s^{-1}$, $k_{2, trans} = 1.1(4) \times 10^{-10} cm^3 \, s^{-1}$ (both values are Ca^+ electronic state averaged) and the ratio $k_{2, cis}/k_{2, trans} = 2.1(5)$ within a 95% confidence interval. This fit also yielded the rotational temperature of the molecules in the beam to be 1.1 K.

D. Variation of Ca⁺ electronic state populations

As described in Sec. II B, Ca^+ ions were constantly excited during laser cooling so that collisions occurred between 3AP and Ca^+ in the $(4s)^2S_{1/2}$, $(3d)^2D_{3/2}$, and $(4p)^2P_{1/2}$ states. To study the effect of the electronic excitation of Ca^+ on the reaction rates, we varied the Ca^+ state populations by changing the detuning of the cooling laser beam from the $(4s) \rightarrow (4p)$ resonance while optimizing the $(3d) \rightarrow (4p)$ repumping laser detuning to achieve the best cooling conditions. Figure 6 shows the measured rate constants as a function of the $(4p)$ state population using an undeflected molecular beam of 3AP molecules.

From this set of measurements, the state-specific rate constants k_2 listed in Table I were derived following the procedures outlined in Refs. 43 and 45. The rate constant for reactions out of the excited $(4p)$ state was found to be two to three orders of magnitude larger than the rate coefficients for reactions out of the $(4s)$ and $(3d)$ states. In the experiments reported in this paper, a detuning of 47–56 MHz was used, yielding a population of the $(4p)$ level of 5%–10%.

Because of its large rate constant, this channel dominates the reaction rates observed in the experiment and the contribution of the other channels can be neglected in good approximation. Thus, one can assume that the conformer-specific rate constants determined in Sec. IV C only reflect reactions with Ca^+ $(4p)$. Scaled to a state population
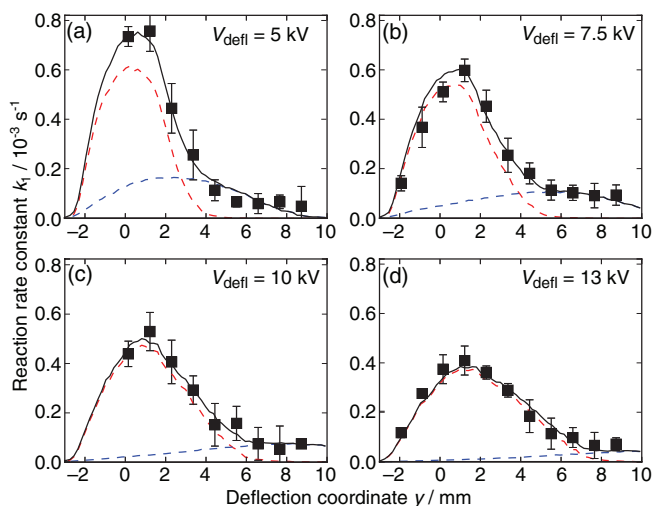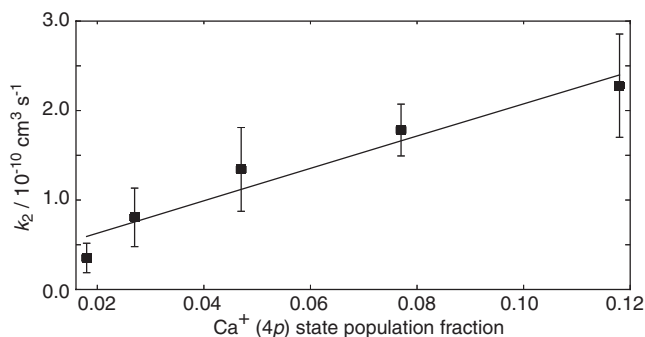

FIG. 5. Reaction profiles (symbols) and their fits (lines) at (a) 5 kV, (b) 7.5 kV, (c) 10 kV, and (d) 13 kV. The solid black lines represent the calculated total contributions of both conformers. Dashed lines represent individual contributions of the *trans* (red) and *cis* (blue) conformers. Error bars indicate the statistical 95% confidence interval of the data points.

FIG. 6. Conformer-averaged bimolecular rate constant k_2 as a function of the population in the Ca^+ $(4p)$ state. Error bars represent the statistical 95% confidence interval. The line represents a linear regression to the data.

TABLE I. Bimolecular rate constants k_2 for reactions of Ca^+ in its relevant electronic states with 3AP molecules in an undeflected beam.

Reaction channel	$k_2 (cm^3 s^{-1})$
$Ca^+(4s)^2S_{1/2}$ + 3AP	$2.66(44) \times 10^{-11}$
$Ca^+(3d)^2D_{3/2}$ + 3AP	$2.69(45) \times 10^{-12}$
$Ca^+(4p)^2P_{1/2}$ + 3AP	$1.91(32) \times 10^{-9}$

of 100%, the conformer-specific second-order rate-constants $k_{2, cis} = 3.2(13) \times 10^{-9} \, cm^3 \, s^{-1}$ and $k_{2, trans} = 1.5(6) \times 10^{-9} \, cm^3 \, s^{-1}$ for the reaction of *cis*-3AP and *trans*-3AP, respectively, with Ca^+ (4p) were obtained.

E. Mass spectra of reaction products

Figures 7(a) and 7(b) show RE mass spectra before and after a typical reaction, respectively. In the spectrum of the pure Ca^+ Coulomb crystal, Figure 7(a), a single peak at an excitation frequency of 140 kHz was observed. This feature was also present in the RE mass spectrum of the multi component crystal after the reaction and could unambiguously be assigned to the excitation of Ca^+ ions with a mass of 40 u. The spectrum of the Coulomb crystal after reaction showed two additional strong peaks at 120 and 165 kHz. The feature at lower frequency was assigned to product ions. MD simulations for crystals composed of 350 Ca^+ and 325 heavier ions indicate that the product ion mass is in the range of 50 to 60 u, suggesting that the reaction products are $CaOH^+$ (57 u) or $CaNH_2^+$ (56 u). As discussed in detail in Refs. 45 and 46, our approximate simulation approach cannot be expected to perfectly reproduce the observed peak positions and intensities in the spectra as it is not a faithful representation of the complex processes leading to the signal measured in the experiments (see Sec. III C). Nonetheless, the MD simulations serve as a useful guide for the interpretation of the mass spectra.

Based on the analysis of the ion trajectories obtained in the MD simulations, the peak at ≈165 kHz was assigned to
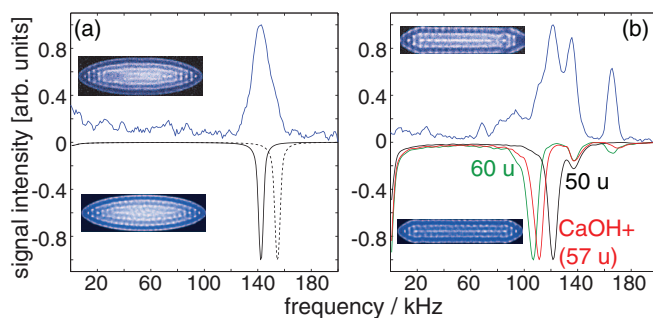

FIG. 7. Resonance-excitation mass spectra (upper traces) and their molecular dynamics simulations (lower inverted traces). (a) Top: experimental spectrum of a pure Ca^+ crystal. Bottom, dashed line: corresponding simulation using a crystal with 675 ions. Solid line: simulated spectrum scaled by 0.92 along the frequency axis to match the experiment. (b) Top: experimental spectra after a reaction time of 8 min with 3AP. Bottom: scaled simulated spectra of crystals composed of 350 Ca^+ and 325 heavy ions with mass 50 u (black), 57 u (red), and 60 u (green).

a high-frequency excitation of Ca^+ ions in the combined potential of the trapping fields and the product ions. The weak broad signal in the range from 60 to 100 kHz is indicative of the presence of even higher masses, possibly arising from consecutive reactions of the primary product ions with 3AP from the molecular beam.

V. REACTION MECHANISMS AND KINETICS

A. Reaction pathways on the ground-state potential energy surface

According to Table I, the Ca^+ (4p) state rate constant is at least two orders of magnitude larger than those in the (4s) and (3d) states, suggesting different reaction dynamics for these channels. The large values for the rate constants obtained for reactions in the Ca^+ (4p) state are indicative of a capture process.[64,65] In this case, the reaction rate is limited by the rate of formation of the reaction complex. Afterward, the reaction proceeds with near unit efficiency. The kinetics of the reaction are then solely controlled by long-range intermolecular interactions. For reactions with Ca^+ (4s) and (3d), however, the significantly smaller rate constants compared to the capture limit are indicative of the existence of barriers on the reaction path which limit the reaction rates.[66,67] In the next paragraphs, the possible roles of the different 3AP conformations in these two types of situations are discussed.

While a high-level *ab initio* calculation for the potential energy surfaces of the excited channels is beyond the scope of the present work, the results of the DFT calculations for the ground-state surface can nonetheless give valuable insights into possible transition-state (TS) structures and reaction pathways. Figure 8 shows a schematic potential energy diagram of stationary points and TS of the $Ca^+(4s)$ + *cis/trans*-3AP reaction. The reactants form the ion-molecule complex C1 in the entrance channel in which Ca^+ is bound above the aromatic ring. From C1, the reaction proceeds either by abstraction of OH or NH_2, yielding the ionic products $CaOH^+$ and $CaNH_2^+$, respectively. For the pathway leading to $CaOH^+$ + 3-aminophenyl radical, the reaction proceeds through TS-CaOH. This TS was found to be identical for both conformers of 3AP as the OH group is displaced from the aromatic ring towards the Ca^+ ion. The resulting products are identical for both conformers. This pathway is calculated to be exothermic by ≈0.3 eV (2320 cm^{-1}).

For the second pathway, leading to $CaNH_2^+$ and *cis/trans*-3-hydroxyphenyl radical, a TS structure TS-CaNH$_2$, analogous to TS-CaOH, was found. The Ca^+ ion is coordinated above the aromatic ring and the amino group is displaced out of the plane towards the ion. Two different TS-structures for the two conformers of 3AP exist. They differ by the orientation of the OH-group with respect to the amino group. Their energy difference was calculated to be 76 cm^{-1}. The conformational dependence is preserved throughout the product channel, but the energy difference between the two conformeric pathways is very small. The pathway leading to $CaNH_2^+$ is calculated to be endothermic by ≈0.72 eV (5800 cm^{-1}). Under the present conditions, this second
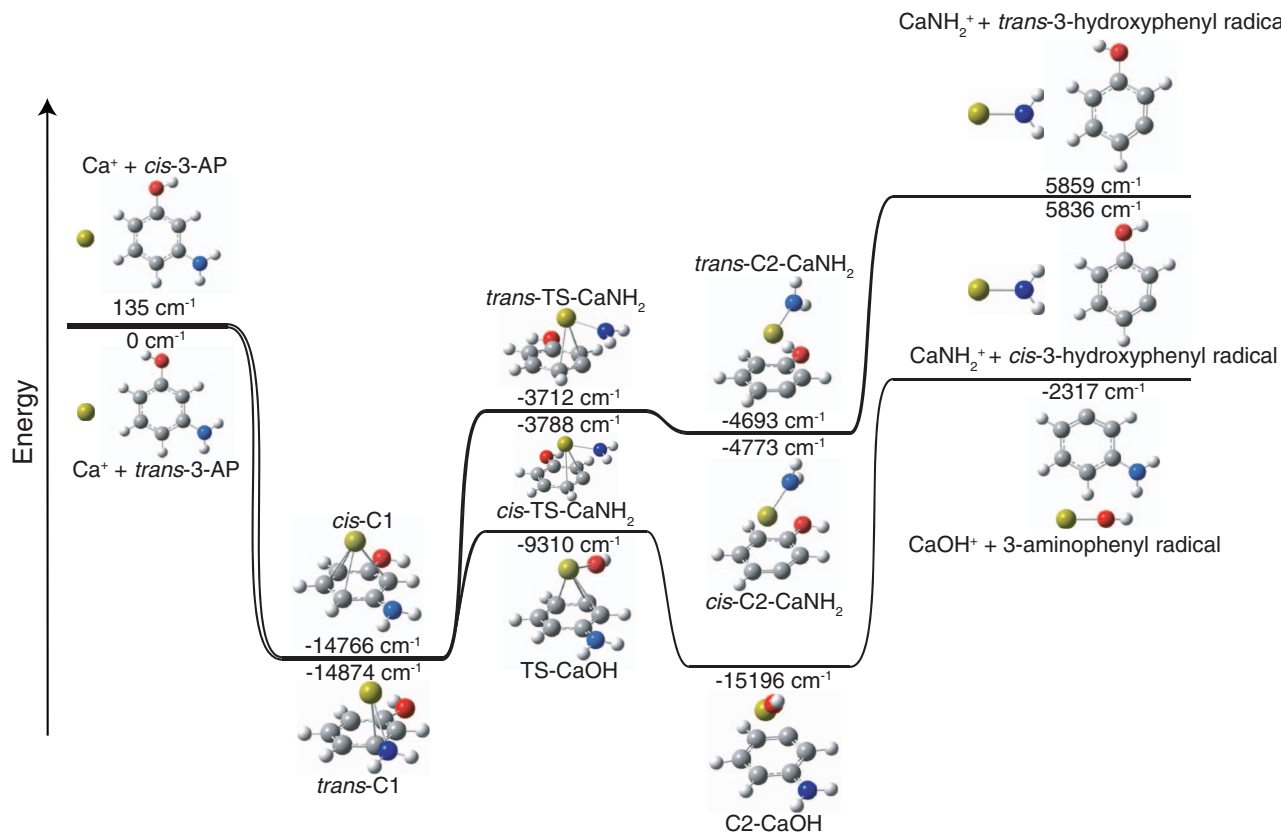
FIG. 8. Schematic energy diagram of stationary points and transition states on the $Ca^+(4s) + cis/trans$-3AP potential energy surface. See text for details.

pathway is expected to be thermodynamically accessible only for reactions with Ca^+ in the excited $(4p)$ and $(3d)$ states.

The present DFT calculations predict that Ca^+ in its ground state reacts with 3AP to $CaOH^+$ via a submerged transition state, TS-CaOH in Figure 8, that is lower in energy than the reagents. The energy profile along the reaction coordinates is reminiscent of the situation in related abstraction reactions, e.g., $Ca^+ + CH_3F$[33,44] or the reactions of O atoms with alkenes.[66,68] The present calculations predict the TS structure to be 1.2 eV lower in energy than the reactants. Comparing with the kinetics in similar type of reactions as observed in Refs. 33, 66, and 68, it is difficult to see how the low-lying barrier in the present case can lead to a rate constant for the Ca^+ $(4s)$ + 3AP channel about two orders of magnitude lower than the capture limit observed (see Sec. IV D). Possible reasons for this discrepancy could be an underestimation of the barrier height by the current DFT approach or the existence of additional barriers or dynamic constraints that have not been accounted for. Overall, the present calculations give no indication of a short-range reaction mechanism that could explain the factor of 2 difference in the observed rate constants for the reaction of $cis/trans$-3AP with Ca^+ in its ground state.

B. Capture dynamics in the Ca^+ $(4p)$+3AP excited channel

Figure 9 shows centrifugally corrected adiabatic potential energy curves for the reaction of Ca^+ $(4p)$ with cis and $trans$-3AP in their $j = 0$ rotational states. In the case of cis-3AP, the centrifugal barrier is more strongly suppressed and reactive collisions proceed up to larger maximum values J_{max} of the total angular momentum. For the collision energy of the present study (0.123 eV), we find $J_{max} = 417$ and 342 for the cis- and $trans$-conformers, respectively. Thus, in a classical picture, a larger impact parameter $b_{max} = J_{max}/\mu v$ results for the cis-conformer, with μ being the reduced mass and v the collision velocity so that a larger reaction cross section $\sigma = \pi b_{max}^2$ is obtained for the cis compared to the $trans$ species.
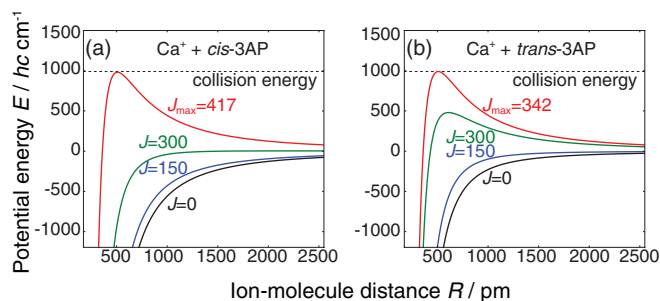

FIG. 9. Centrifugally corrected long-range interaction potentials for (a) cis- and (b) $trans$-3AP in the rotational ground state $j = 0$. Reprinted with permission from Y.-P. Chang, K. Długołęcki, J. Küpper, D. Rösch, D. Wild, and S. Willitsch, "Specific chemical reactivities of spatially separated 3-aminophenol conformers with cold Ca^+ ions," Science **342**, 98–101 (2013). Copyright 2013 AAAS.[29]
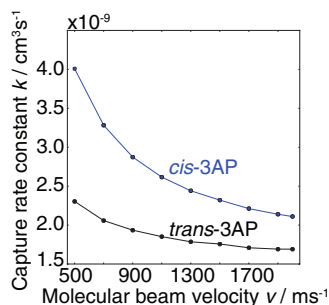
FIG. 10. Capture rate constants of *cis*- and *trans*-3AP in the rotational quantum state $j = 0$ as a function of the collision velocity. The experimental collision velocity amounted to $v = 900$ ms^{-1}.

VI. SUMMARY AND CONCLUSIONS

We have presented a new method for the characterization of conformer-specific chemical reactivities. In a proof-of-concept study, the two conformers of 3AP were spatially separated in a molecular beam using the electrostatic deflector. Subsequently, the separated conformers reacted with a stationary target of Coulomb-crystallized, laser-cooled Ca$^+$ ions. Second-order rate constants for the reactions of the individual conformers with Ca$^+$ were obtained. The reaction rate for the *cis* conformer was found to be a factor of two larger than that for the *trans* conformer. A detailed analysis of the rate constants for the individual electronic states of Ca$^+$ showed that the observed reaction rates are dominated by the reaction of 3AP with electronically excited Ca$^+$ ($4p$). The reaction rates of 3AP with Ca$^+$ in its $(4s)^2 S_{1/2}$ ground and $(3d)^2 D_{3/2}$ excited states were found to be two to three orders of magnitude smaller. CaOH$^+$ and CaNH$_2^+$ were identified as the likely reaction products by resonant-excitation mass spectrometry.

The rate constant observed for the Ca$^+$ ($4p$) reaction channel was found to be close to the capture limit. The difference in the reactivities of the two conformers could be rationalized in terms of adiabatic-capture theory in very good agreement with the experimental findings. Within the capture picture, the increased reaction rate for the *cis* conformer compared to the *trans* species is explained by the stronger ion-dipole long-range interaction which results in a larger capture cross section. The small reaction rates with Ca$^+$ in its ($4s$) and ($3d$) states indicate the existence of dynamic bottlenecks along the reaction path. Preliminary DFT calculations for the reaction of 3AP with Ca$^+$ on the ground state potential energy surface enabled a first characterization of possible reaction pathways. However, more extensive computations are necessary to elucidate the short-range dynamics in all three reaction channels probed in the present experiments.

We expect that the present technique of combining electrostatic conformer selection with highly sensitive Coulomb-crystal methods will enable the study of conformational effects in a range of ion-molecule reactions. Electrostatic conformer separation is applicable to a variety of polar molecules as long as their conformers exhibit appreciably different dipole moments. More advanced techniques for the separation of molecular species and individual quantum states using electric field manipulation have been reported and could be implemented in the current methodology.[26, 69–72] For the ionic reaction partners, the generation of Coulomb crystals of sympathetically cooled ions allows the study of a wide range of atomic and molecular ionic species.[30] Moreover, the preparation of Coulomb crystals with molecular ions in selected internal quantum states has been recently accomplished[73, 74] so that simultaneous studies of conformational and state-specific effects are now within reach for a wide range of ion-molecule reactions.

As shown in Figure 10, the calculated capture rate constants depend on the collision energy. Moreover, the monotonic increase of rate constants with decreasing collision energy is more prominent for the *cis* species with the larger dipole moment. Therefore, the ratio of the reactivity between the two conformers becomes larger for smaller collisional energies. We also investigated the dependence of the capture rate constants on the rotational state of 3AP. As exemplified for the *cis* conformer at the experimental collision energy in Figure 11(a), the capture rates slightly decrease as j increases. Since the rotational temperature is about 1.1 K, about 90% of the 3AP population is confined to the rotational states $j = 1$–5 for which the relative difference of the rate constants is <10%. Figure 11(b) shows the dependence of the capture rate constant for the *cis* conformer on the asymmetric-top quantum number τ. The dependence is only weak over the range of states $j = 0$–5.

By averaging over capture rate constants of all populated rotational states of 3AP at 1.1 K and for a collision energy of 0.123 eV, one obtains the effective capture rate constants $k_{2,\,cis} = 2.7 \times 10^{-9}$ cm^3 s^{-1} and $k_{2,\,trans} = 1.8 \times 10^{-9}$ cm^3 s^{-1} and their ratio $k_{2,\,cis}/k_{2,\,trans} = 1.5$. These values are in good agreement with the experimentally observed second-order rate constants for the reaction with Ca$^+$ in the excited ($4p$) state, see Sec. IV D.
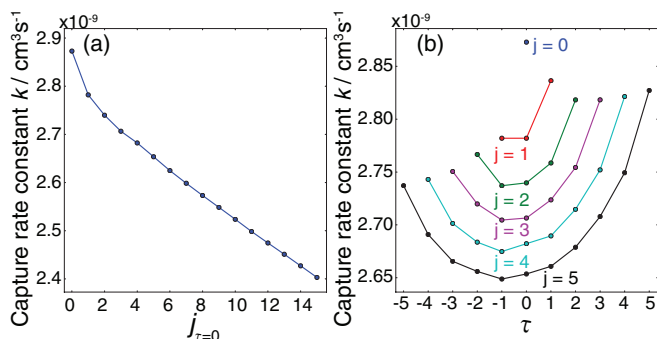
ACKNOWLEDGMENTS

FIG. 11. State-dependent capture rate constants k for *cis*-3-aminophenol. (a) Dependence on rotational state $j(\tau = 0)$ for $j = 0$ to $j = 15$. (b) Dependence on the asymmetric-top quantum number τ for $j = 0$ to $j = 5$. Lines are drawn to guide the eye. See text for details.

[1] D. H. R. Barton, "The stereochemistry of cyclohexane derivatives," J. Chem. Soc. **1953**, 1027.

[2] H. C. Dunathan, "Conformation and reaction specificity in pyridoxal phosphate enzymes," Proc. Natl. Acad. Sci. U.S.A. **55**, 712–716 (1966).

[3] E. L. Eliel and S. H. Wilen, *Stereochemistry of Organic Compounds* (John Wiley & Sons, New York, USA, 1994).

[4] R. D. Suenram and F. J. Lovas, "Millimeter wave spectrum of glycine—a new conformer," J. Am. Chem. Soc. **102**, 7180–7184 (1980).

[5] T. R. Rizzo, Y. D. Park, L. A. Peteanu, and D. H. Levy, "The electronic spectrum of the amino acid tryptophan in the gas phase," J. Chem. Phys. **84**, 2534–2541 (1986).

[6] E. G. Robertson and J. P. Simons, "Getting into shape: Conformational and supramolecular landscapes in small biomolecules and their hydrated clusters," Phys. Chem. Chem. Phys. **3**, 1–18 (2001).

[7] R. Weinkauf, J. Schermann, M. S. de Vries, and K. Kleinermanns, "Molecular physics of building blocks of life under isolated or defined conditions," Eur. Phys. J. D **20**, 309–316 (2002).

[8] J. P. Simons, "Bio-active molecules in the gas phase," Phys. Chem. Chem. Phys. **6**, E7–E7 (2004).

[9] J. P. Simons, R. A. Jockusch, P. Çarçabal, I. Hünig, R. T. Kroemer, N. A. Macleod, and L. C. Snoek, "Sugars in the gas phase. Spectroscopy, conformation, hydration, co-operativity and selectivity," Int. Rev. Phys. Chem. **24**, 489 (2005).

[10] M. S. de Vries and P. Hobza, "Gas-phase spectroscopy of biomolecular building blocks," Annu. Rev. Phys. Chem. **58**, 585–612 (2007).

[11] M. E. Sanz, S. Blanco, J. C. Lopez, and J. L. Alonso, "Rotational probes of six conformers of neutral cysteine," Angew. Chem., Int. Ed. **47**, 6216–6220 (2008).

[12] T. R. Rizzo, J. A. Stearns, and O. V. Boyarkin, "Spectroscopic studies of cold, gas-phase biomolecular ions," Int. Rev. Phys. Chem. **28**, 481 (2009).

[13] N. S. Nagornova, T. R. Rizzo, and O. V. Boyarkin, "Interplay of intra- and intermolecular H-bonding in a progressively solvated macrocyclic peptide" Science **336**, 320–323 (2012).

[14] B. C. Dian, A. Longarte, and T. S. Zwier, "Conformational dynamics in a dipeptide after single-mode vibrational excitation," Science **296**, 2369–2373 (2002).

[15] B. C. Dian, J. R. Clarkson, and T. S. Zwier, "Direct measurement of energy thresholds to conformational isomerization in tryptamine," Science **303**, 1169–1173 (2004).

[16] B. C. Dian, G. G. Brown, K. O. Douglass, and B. H. Pate, "Measuring picosecond isomerization kinetics via broadband microwave spectroscopy," Science **320**, 924–928 (2008).

[17] S. T. Park and M. S. Kim, "Photodissociation dynamics of various conformers of iodobutane isomer ions prepared selectively by vacuum ultraviolet mass-analyzed threshold ionization," J. Am. Chem. Soc. **124**, 7614–21 (2002).

[18] S. T. Park, S. K. Kim, and M. S. Kim, "Observation of conformer-specific pathways in the photodissociation of 1-iodopropane ions," Nature (London) **415**, 306 (2002).

[19] M. H. Kim, L. Shen, H. Tao, T. J. Martinez, and A. G. Suits, "Conformationally controlled chemistry: exited-state dynamics dictate ground-state reaction," Science **315**, 1561 (2007).

[20] T. A. A. Oliver, G. A. King, and M. N. R. Ashfold, "The ultraviolet photodissociation of axial and equatorial conformers of 3-pyrroline," J. Chem. Phys. **133**, 194303 (2010).

[21] T. A. A. Oliver, G. A. King, and M. N. R. Ashfold, "The conformer resolved ultraviolet photodissociation of morpholine," Chem. Sci. **1**, 89 (2010).

[22] D. K. Zaouris, A. M. Wenge, D. Murdock, T. A. A. Oliver, G. Richmond, G. A. D. Ritchie, R. N. Dixon, and M. N. R. Ashfold, "Conformer specific dissociation dynamics of iodocyclohexane studied by velocity map imaging" J. Chem. Phys. **135**, 094312 (2011).

[23] C. A. Taatjes, O. Welz, A. J. Eskola, J. D. Savee, A. M. Scheer, D. E. Shallcross, B. Rotavera, E. P. F. Lee, J. M. Dyke, D. K. W. Mok, D. L. Osborn, and C. J. Percival, "Direct measurements of conformer-dependent reactivity of the Criegee iIntermediate CH_3CHOO," Science **340**, 177 (2013).

[24] L. Khriachtchev, A. Domanskaya, K. Marushkevich, M. Räsänen, B. Grigorenko, A. Ermilov, N. Andrijchenko, and A. Nemukhin, "Conformation-dependent chemical reaction of formic acid with an oxygen atom," J. Phys. Chem. A **113**, 8143 (2009).

[25] G. von Helden, T. Wyttenbach, and M. T. Bowers, "Conformation of macromolecules in the gas-phase—use of matrix-assisted laser-desorption methods in ion chromatography," Science **267**, 1483–1485 (1995).

[26] F. Filsinger, U. Erlekam, G. von Helden, J. Küpper, and G. Meijer, "Selector for structural isomers of neutral molecules," Phys. Rev. Lett. **100**, 133003 (2008); e-print arXiv:0802.2795 [physics].

[27] F. Filsinger, J. Küpper, G. Meijer, J. L. Hansen, J. Maurer, J. H. Nielsen, L. Holmegaard, and H. Stapelfeldt, "Pure samples of individual conformers: the separation of stereo-isomers of complex molecules using electric fields," Angew. Chem., Int. Ed. **48**, 6900–6902 (2009).

[28] T. Kierspel, D. A. Horke, Y.-P. Chang, and J. Küpper, "Spatially separated polar samples of the cis and trans conformers of 3-fluorophenol," Chem. Phys. Lett. **591**, 130–132 (2014); e-print arXiv:1312.4417 [physics].

[29] Y.-P. Chang, K. Długołęcki, J. Küpper, D. Rösch, D. Wild, and S. Willitsch, "Specific chemical reactivities of spatially separated 3-aminophenol conformers with cold Ca^+ ions," Science **342**, 98–101 (2013); e-print arXiv:1308.6538 [physics].

[30] S. Willitsch, Int. Rev. Phys. Chem. **31**, 175 (2012).

[31] K. Eller and H. Schwarz, "Organometallic chemistry in the gas phase," Chem. Rev. **91**, 1121–1177 (1991).

[32] H. Schwarz, "Chemistry with methane: Concepts rather than recipes," Angew. Chem., Int. Ed. **50**, 10096 (2011).

[33] J. N. Harvey, D. Schröder, W. Koch, D. Danovich, S. Shaik, and H. Schwarz, "Electron-transfer reactivity in the activation of organic fluorides by bare metal monocations," Chem. Phys. Lett. **273**, 164 (1997).

[34] X. Zhao, G. K. Koyanagi, and D. K. Bohme, "Reactions of methyl fluoride with atomic transition-metal and main-group cations: Gas-phase room-temperature kinetics and periodicities in reactivity," J. Phys. Chem. A **110**, 10607 (2006).

[35] V. Ryzhov and R. C. Dunbar, "Interactions of phenol and indole with metal ions in the gas phase: Models for Tyr and Trp side-chain binding," J. Am. Chem. Soc. **121**, 2259–2268 (1999).

[36] F. Filsinger, J. Küpper, G. Meijer, L. Holmegaard, J. H. Nielsen, I. Nevo, J. L. Hansen, and H. Stapelfeldt, "Quantum-state selection, alignment, and orientation of large molecules using static electric and laser fields," J. Chem. Phys. **131**, 064309 (2009); e-print arXiv:0903.5413 [physics].

[37] S. Willitsch, M. T. Bell, A. D. Gingell, and T. P. Softley, "Chemical applications of laser- and sympathetically-cooled ions in ion traps," Phys. Chem. Chem. Phys. **10**, 7200 (2008).

[38] U. Even, J. Jortner, D. Noy, N. Lavie, and N. Cossart-Magos, "Cooling of large molecules below 1 K and He clusters formation," J. Chem. Phys. **112**, 8068–8071 (2000).

[39] H. K. Hughes, "The electric resonance method of radiofrequency spectroscopy the moment of inertia and electric dipole moment of CsF," Phys. Rev. **72**, 614–623 (1947).

[40] C. A. Lee, B. P. Fabricand, R. O. Carlson, and I. I. Rabi, "Molecular beam investigation of rotational transitions. 1. The rotational levels of KCl and their hyperfine structure," Phys. Rev. **91**, 1395–1403 (1953).

[41] N. F. Ramsey, *Molecular Beams*, The International Series of Monographs on Physics (Oxford University Press, London, 1956); reprinted in *Oxford Classic Texts in the Physical Sciences* (2005).

[42] L. Holmegaard, J. H. Nielsen, I. Nevo, H. Stapelfeldt, F. Filsinger, J. Küpper, and G. Meijer, "Laser-induced alignment and orientation of quantum-state-selected large molecules," Phys. Rev. Lett. **102**, 023001 (2009); e-print arXiv:0810.2307 [physics].

[43] F. H. J. Hall, M. Aymar, N. Bouloufa-Maafa, O. Dulieu, and S. Willitsch, "Light-assisted ion-neutral reactive processes in the cold regime: Radiative molecule formation versus charge exchange," Phys. Rev. Lett. **107**, 243202 (2011); e-print arXiv:1301.0724 [physics].

[44] S. Willitsch, M. T. Bell, A. D. Gingell, S. R. Procter, and T. P. Softley, "Cold reactive collisions between laser-cooled ions and velocity-selected neutral molecules," Phys. Rev. Lett. **100**, 043203 (2008).

[45] F. H. Hall, P. Eberle, G. Hegi, M. Raoult, M. Aymar, O. Dulieu, and S. Willitsch, "Ion-neutral chemistry at ultralow energies: dynamics of reactive collisions between laser-cooled Ca^+ ions and Rb atoms in an ion-atom hybrid trap," Mol. Phys. **111**, 2020–2032 (2013); e-print arXiv:1302.4682 [physics].

[46] B. Roth, P. Blythe, and S. Schiller, "Motional resonance coupling in cold multispecies Coulomb crystals," Phys. Rev. A **75**, 023402 (2007).

[47] J. A. Reese, T. V. Nguyen, T. M. Korter, and D. W. Pratt, "Charge redistribution on electronic excitation. Dipole moments of *cis* and *trans-3-*aminophenol in their S_0 and S_1 electronic states," J. Am. Chem. Soc. **126**, 11387–11392 (2004).

[48] M. J. Frisch, G. W. Trucks, H. B. Schlegel *et al.*, Gaussian 09, Revision A.02, Gaussian, Inc., Wallingford, CT, 2009.

[49] B. J. Lynch, P. L. Fast, M. Harris, and D. G. Truhlar, "Adiabatic connection for kinetics," J. Phys. Chem. A **104**, 4811 (2000).

[50] T. H. Dunning, "Gaussian basis sets for use in correlated molecular calculations. I. The atoms boron through neon and hydrogen," J. Chem. Phys. **90**, 1007 (1989).

[51] C. Peng and H. B. Schlegel, "Combining synchronous transit and quasi-Newton methods to find transition states," Isr. J. Chem. **33**, 449 (1993).

[52] C. Peng, P. Y. Ayala, H. B. Schlegel, and M. J. Frisch, "Using redundant internal coordinates to optimize equilibrium geometries and transition states," J. Comput. Chem. **17**, 49–56 (1996).

[53] D. C. Clary, "Calculations of rate constants for ion-molecule reactions using a combined capture and centrifugal sudden approximation," Mol. Phys. **54**, 605 (1985).

[54] T. Stoecklin, D. C. Clary, and A. Palma, "Rate constant calculations for ion-symmetric top and ion-asymmetric top reactions," J. Chem. Soc., Faraday Trans. **88**, 901 (1992).

[55] Here, "permanent dipole" refers to the dipole moment of 3AP in its molecular frame.[75]

[56] F. Filsinger, K. Wohlfart, M. Schnell, J.-U. Grabow, and J. Küpper, "Precise dipole moments and quadrupole coupling constants of the *cis* and *trans* conformers of 3-aminophenol: Determination of the absolute conformation," Phys. Chem. Chem. Phys. **10**, 666–673 (2008); e-print arXiv:0708.0282 [physics].

[57] T. Matthey, T. Cickovski, S. Hampton, A. Ko, Q. Ma, M. Nyerges, T. Raeder, T. Slabach, and J. A. Izaguirre, "Protomol, an object-oriented framework for prototyping novel algorithms for molecular dynamics," ACM Trans. Math. Softw. **30**, 237–265 (2004).

[58] M. T. Bell, A. D. Gingell, J. Oldham, T. P. Softley, and S. Willitsch, "Ion-molecule chemistry at very low temperatures: cold chemical reactions between coulomb-crystallized ions and velocity-selected neutral molecules," Faraday Discuss. **142**, 73 (2009).

[59] J. Küpper, F. Filsinger, and G. Meijer, "Manipulating the motion of large molecules," Faraday Discuss. **142**, 155–173 (2009); e-print arXiv:0906.4355 [physics].

[60] Y.-P. Chang, F. Filsinger, B. Sartakov, and J. Küpper, "CMIstark: Python package for the stark-effect calculation and symmetry classification of linear, symmetric and asymmetric top wavefunctions in dc electric fields," Comput. Phys. Commun. **185**, 339–349 (2014); e-print arXiv:1308.4076 [physics].

[61] J. M. C. Plane, T. Vondrak, S. Broadley, B. Cosic, A. Ermoline, and A. Fontijn, "Kinetic study of the reaction $Ca^+ + N_2O$ from 188 to 1207 K," J. Phys. Chem. A **110**, 7874 (2006).

[62] J. S. Chickos and W. E. Acree, "Enthalpies of sublimation of organic and organometallic compounds. 1910–2001," J. Phys. Chem. Ref. Data **31**, 537 (2002).

[63] For 3AP, the number density in each gas pulse n_{pulse} is equal to 2.56(41) $\times 10^8$ cm^{-3}. n_{avg} equals to a product of the gas pulse duration (50 μs), the repetition rate (600 Hz), and n_{pulse}.

[64] B. R. Rowe and J. B. Marquette, "CRESU studies of ion/molecule reactions," Int. J. Mass Spectrom. Ion Processes **80**, 239 (1987).

[65] D. Clary, "Fast chemical reactions: Theory challenges experiment," Annu. Rev. Phys. Chem. **41**, 61–90 (1990).

[66] H. Sabbah, L. Biennier, I. R. Sims, Y. Georgievskii, S. J. Klippenstein, and I. W. M. Smith, "Understanding reactivity at very low temperatures: the reactions of oxygen atoms with alkenes," Science **317**, 102–105 (2007).

[67] A. D. Gingell, M. T. Bell, J. M. Oldham, T. P. Softley, and J. N. Harvey, "Cold chemistry with electronically excited Ca^+ Coulomb crystals" J. Chem. Phys. **133**, 194302 (2010).

[68] I. W. M. Smith, A. M. Sage, N. M. Donahue, E. Herbst, and D. Quan, "The temperature-dependence of rapid low temperature reactions: experiment, understanding and prediction," Faraday Discuss. **133**, 137 (2006).

[69] J. H. Nielsen, P. Simesen, C. Z. Bisgaard, H. Stapelfeldt, F. Filsinger, B. Friedrich, G. Meijer, and J. Küpper, "Stark-selected beam of ground-state OCS molecules characterized by revivals of impulsive alignment," Phys. Chem. Chem. Phys. **13**, 18971–18975 (2011); e-print arXiv:1105.2413 [physics].

[70] S. Putzke, F. Filsinger, H. Haak, J. Küpper, and G. Meijer, "Rotational-state-specific guiding of large molecules," Phys. Chem. Chem. Phys. **13**, 18962 (2011); e-print arXiv:1103.5080 [physics].

[71] S. Trippel, Y.-P. Chang, S. Stern, T. Mullins, L. Holmegaard, and J. Küpper, "Spatial separation of state- and size-selected neutral clusters," Phys. Rev. A **86**, 033202 (2012); e-print arXiv:1208.4935 [physics].

[72] S. Y. T. van de Meerakker, H. L. Bethlem, N. Vanhaecke, and G. Meijer, "Manipulation and control of molecular beams," Chem. Rev. **112**, 4828–4878 (2012).

[73] X. Tong, A. H. Winney, and S. Willitsch, "Sympathetic cooling of molecular ions in selected rotational and vibrational states produced by threshold photoionization," Phys. Rev. Lett. **105**, 143001 (2010); e-print arXiv:1006.5642 [physics].

[74] X. Tong, D. Wild, and S. Willitsch, "Collisional and radiative effects in the state-selective preparation of translationally cold molecular ions in ion traps," Phys. Rev. A **83**, 023415 (2011).

[75] W. Klemperer, K. K. Lehmann, J. K. G. Watson, and S. C. Wofsy, "Can molecules have permanent electric dipole moments?" J. Phys. Chem. **97**, 2413–2416 (1993).